Intestinal Epithelial Apoptosis initiates Gut Mucosal Injury during Extracorporeal Membrane Oxygenation in the Newborn Piglet

Krishnan MohanKumar[1,2], **Cheryl R. Killingsworth**[3], **R. Britt McILwain**[4], **Joseph G. Timpa**[4], **Ramasamy Jagadeeswaran**[1,2], **Kopperuncholan Namachivayam**[1,2], **Ashish R. Kurundkar**[5], **David R. Kelly**[5], **Steven A. Garzon**[6], and **Akhil Maheshwari**[1,2,7]

[1]Department of Pediatrics, Division of Neonatology, University of Illinois at Chicago, 840 S Wood St, CSB 1257, Chicago, IL 60612

[2]Department of Pediatrics, Center for Neonatal and Pediatric Gastrointestinal Disease, University of Illinois at Chicago, 840 S Wood St, CSB 1257, Chicago, IL 60612

[3]Animal Resources Program, University of Alabama at Birmingham (UAB), 619 South 19th St, Birmingham, AL 35233

[4]University Hospital Services, University of Alabama at Birmingham (UAB), 619 South 19th St, Birmingham, AL 35233

[5]Department of Pathology, University of Alabama at Birmingham (UAB), 619 South 19th St, Birmingham, AL 35233

[6]Department of Pathology, University of Illinois at Chicago, 840 S Wood St, CSB 1257, Chicago, IL 60612

[7]Department of Pharmacology, University of Illinois at Chicago, 840 S Wood St, CSB 1257, Chicago, IL 60612

Abstract

Background—Neonates and young infants exposed to extracorporeal circulation during extracorporeal membrane oxygenation (ECMO) and cardiopulmonary bypass (CPB) are at risk of developing a systemic inflammatory response syndrome (SIRS) with multi-organ dysfunction. We used a piglet model of ECMO to investigate the hypothesis that epithelial apoptosis is an early event that precedes villous damage during ECMO-related bowel injury.

Methods—Healthy 3-week-old piglets were subjected to ECMO for up to 8h. Epithelial apoptosis was measured in histopathological analysis, nuclear imaging, and terminal

Address for correspondence: Akhil Maheshwari, MD, 840 S Wood St, CSB 1257, UIC m/c 856, Chicago, IL 60612, Phone: 312-996-4185, Fax: 312-355-5548, akhil1@uic.edu.

deoxynucleotidyl transferase dUTP nick end labeling. Plasma intestinal-fatty acid-binding protein (I-FABP) levels were measured by enzyme immunoassay. Intestinal mast cells were isolated by fluorescence-assisted cell sorting. Cleaved caspase-8, caspase-9, phospho-p38 MAPK, and fas ligand expression was investigated by immunohistochemistry, Western blots, and reverse transcriptase-quantitative polymerase chain reaction.

Results—Piglet ECMO was associated with increased gut epithelial apoptosis. Extensive apoptotic changes were noted on villus tips and in scattered crypt cells after 2h of ECMO. After 8h, the villi were denuded and apoptotic changes were evident in a majority of crypt cells. Increased circulating I-FABP levels, a marker of gut epithelial injury, showed that epithelial injury occurred during ECMO. We detected increased cleaved caspase-8, but not cleaved caspase-9, in epithelial cells indicating that the extrinsic apoptotic pathway was active. ECMO was associated with increased *fas* ligand expression in intestinal mast cells, which was induced through activation of the p38 mitogen-activated protein kinase.

Conclusions—Epithelial apoptosis is an early event that initiates gut mucosal injury in a piglet model of ECMO.

Keywords

extracorporeal circulation; mucosal injury; apoptotic; neonate; ECMO

INTRODUCTION

Neonates and young infants exposed to extracorporeal circulation during extracorporeal membrane oxygenation (ECMO) and cardiopulmonary bypass (CPB) are at high risk of developing a systemic inflammatory response syndrome (SIRS) with multi-organ dysfunction.[1–4] CPB is used frequently during cardiothoracic surgery to obtain a non-beating, bloodless heart, whereas ECMO is a life-support system of last resort used to provide oxygenation and/or circulatory support in infants with intractable cardiorespiratory failure due to diverse causes such as persistent pulmonary hypertension of the newborn, meconium aspiration syndrome, sepsis, and heart defects.[5] Understanding ECMO/CPB-related SIRS is critical for the development of anti-inflammatory strategies that may reduce associated morbidity.

To investigate the mechanisms of extracorporeal circulation-related SIRS, we have developed a porcine neonatal model of ECMO where we subject previously-healthy, 3–6 kg piglets to venoarterial ECMO.[6, 7] Piglet ECMO is associated with inflammatory changes similar to those reported in human studies, including hemodynamic changes, leukocyte activation, increased expression of inflammatory cytokines, and microvascular injury in diverse organs such as lung, intestine, liver, and kidney.[6] In this model, disruption of the intestinal epithelial barrier, histopathological evidence of epithelial damage, and bacterial translocation are prominent findings. However, it remains unknown whether the observed loss of intestinal epithelium underlies the gross tissue necrosis, or only coincides with the widespread gut mucosal injury during ECMO. In this study, we investigated the hypothesis that epithelial apoptosis is an early event that precedes villous damage during ECMO-related gut mucosal injury.

METHODS

Neonatal Piglet ECMO

Mixed-breed neonatal piglets of either gender weighing 3–6 kg were subjected to venoarterial ECMO as previously described.[6, 7] Animal studies were performed at University of Alabama at Birmingham after approval by the Institutional Animal Care and Use Committee. During ECMO, the piglets received general anesthesia and mechanical ventilation (volume-controlled, tidal volume 10–15 mL/kg, 10–15 cycles/min, FiO2=21%; Hallowell EMC 2000 ventilator) to maintain acceptable arterial blood gases (pO_2 = 70–150 mmHg, pCO_2 = 35–45 mmHg, and pH = 7.35–7.45). Biomedicus 8F cannulae (Medtronic, Minneapolis, MN) were inserted into the external jugular vein and the external carotid artery. Animals were heparinized to maintain activated clotting times of 180–220 seconds. The ECMO system consisted of a Biomedicus BP-50 centrifugal pump (Medtronic, Shoreview, MN) and a Minimax hollow fiber oxygenator (Medtronic). Gas flow rates were maintained in the oxygenator at 0.5 L/min 100% oxygen. After starting ECMO, flow rates in the circuit were advanced to 250 mL/min or 1.5 L/min/m^2. Sham animals received anesthesia, ventilation, cannulation, and heparinization similar to ECMO animals, but were not connected to the circulatory pump device. Data in this study represent 5 animals each in sham and ECMO groups that were sacrificed after 2h, and 8 animals each in sham and ECMO groups sacrificed after 8h.

Nuclear morphology

Tissue sections were deparaffinized using the EZ-AR common solution (Biogenex, San Remon, CA) per manufacturer's protocol and nuclear staining was obtained with 4′,6-diamidino-2-phenylindole (DAPI; 1:1000 × 3 min; Calbiochem, San Diego, CA). Nuclei with apoptotic changes such as chromatin condensation and/or fragmentation[8] were enumerated using a Zeiss Axiovert fluorescence microscope. Chromatin condensation was defined as coalescence of chromatin into distinct clumps localized mostly at the nuclear periphery and resulting in central 'cavitation'. We also performed nuclear morphological analysis using a previously-described software plugin[9] for Image J, a public-domain image processing program developed at the National Institutes of Health.[10] We measured nuclear area, aspect (ratio between the major and minor radii of the nucleus), area/box (ratio between nuclear area and the area of its bounding box), radius ratio (ratio between the maximum and the minimum nuclear radii), and roundness (computed as perimeter^2/(4 × π × area), where π is the mathematical constant.[9] Nuclear irregularity index (NII) was defined as [aspect − (area/box) + radius ratio + roundness].[9] In this analysis, decreased nuclear area and lower values of the NII are associated with apoptosis.

Terminal deoxynucleotidyl transferase-mediated dUTP Nick End Labeling (TUNEL)

TUNEL staining was performed to detect apoptotic changes in the sham and ECMO intestine. We used a commercially-available kit (Roche, Indianapolis, IN) per manufacturer's instructions. Briefly, deparaffinized sections were treated with proteinase K (15 μg/mL) × 15 min and then rinsed with PBS. Endogenous peroxidase was inactivated by immersing in 3% H_2O_2 × 5 min. Sections were then immersed in a buffer containing deoxynucleotidyl transferase and fluorescein-deoxy-Uridine triphosphate × 90 min at 37°C

in 100% relative humidity. After washing with PBS, the sections were incubated with an Alexa fluor 488-conjugated anti-fluorescein antibody × 30 min. Imaging was performed using the Zeiss Laser scanning microscope (LSM) 510-Meta microscope.

Severity of epithelial cell apoptosis and villous disruption

Serial tissue sections stained with H&E and for TUNEL were scored by a blinded observer for the severity of epithelial cell apoptosis and villous damage, respectively. In TUNEL-stained sections, score 0 = intact villous epithelium, sporadic TUNEL$^+$ nuclei; 1 = clusters of TUNEL$^+$ nuclei on villus tips; 2 = TUNEL$^+$ nuclei covering the villus but not seen in crypts; 3 = TUNEL$^+$ nuclei penetrating into the crypts; and 4 = TUNEL$^+$ nuclei all along the crypt-villus axis.[11] Villous damage was scored similarly: score 0 = intact villi; 1 = sloughing of cells on villus tips; 2 = mid-villus damage; 3 = loss of villi but crypts can be recognized; and 4 = both villi and crypts cannot be recognized. Ten fields were examined per section (n = 5 animals/group) and highest scores were recorded in each microscopic field.

Immunohistochemistry

We used our previously-described protocol for immunohistochemistry.[6, 7] Briefly, tissue sections were deparaffinized, treated with Proteinase K (20 µg/mL) (Promega, Madison, WI) × 10 min, rinsed in PBS × 5 min, and then immersed in blocking buffer (SuperBlock T20 solution; Thermo Scientific, Rockford, IL) × 30 min. Sections were then incubated overnight at 4°C in appropriate primary antibody: *fas* Ligand, c-kit/CD117 (Santa Cruz Biotech, Santa Cruz, CA), cleaved caspase-8 and cleaved caspase-9 (Cell Signaling, Danvers, MA). Secondary staining was performed with Alexa 488 or Alexa 546-conjugated IgG antibody (Invitrogen, San Diego, CA) × 30 min. Controls included slides with no primary antibody and/or with isotype control. Cell nuclei were stained with DAPI. Imaging was performed using the Zeiss LSM 510-Meta confocal microscope.

Western blots

We used our previously-described immunoblotting protocol[6, 7] to measure cleaved caspase-8 and cleaved caspase-9 in sham/ECMO intestine, and phospho-p38 mitogen-activated protein kinase (MAPK; thr180/tyr182) in mast cells (antibodies from Cell Signaling).

Enzyme-linked immunosorbent assay (ELISA)

Plasma intestinal-fatty acid binding protein (I-FABP) concentrations were measured using a commercially-available ELISA kit (MyBioSource, San Diego, CA) per manufacturer's protocol. The assay has a linear range of 78–5000 pg/mL.

Reverse transcriptase-quantitative polymerase chain reaction (RT-qPCR)

Messenger RNA expression of death receptor ligands was quantified using our previously-described SYBR green protocol. Primers were designed using the Beacon Design software (Bio-Rad, Hercules, CA; Table 1). Data were analyzed using the $2^{-\Delta\Delta CT}$ method.

Porcine intestinal mast cells

Intestinal c-kit$^+$ FcεR1$^+$ mast cells were isolated by FACS sorting.[12] Briefly, intestinal tissue was rinsed with Hanks' balanced-salt solution (HBSS) containing 1 mM DTT (Sigma-Aldrich, St. Louis, MO) to remove adherent mucus, washed with HBSS containing 1 mM ethylenediaminetetraacetic acid (Sigma) × 20 min × 2 cycles at 37°C, and then incubated in HBSS containing 1 mM collagenase type IV (Sigma) × 2h at 37°C. Cell suspensions were stained using FITC-conjugated monoclonal anti-human c-kit/CD117 (BD Biosciences, San Jose, CA) and PE-conjugated anti-human FcεR1 antibodies (MyBiosource, San Diego, CA) and dual-positive cells were sorted by FACS. Phospho-p38 MAPK was measured in mast cells by FACS after permeabilizing (Cytofix/Cytoperm kit, BD Biosciences) and staining these cells with PE-conjugated mouse anti-p38 MAPK (thr180/tyr182; BD Biosciences). In some experiments, we treated mast cells with *E. coli* LPS (0.1–1 μg/mL) and/or the p38 inhibitor SB202190 (Sigma) overnight and measured *fas* ligand expression by RT-qPCR.

Statistical methods

Parametric and non-parametric tests were applied using the Sigma Stat 3.1.1 software (Systat, Point Richmond, CA). For PCR data, crossing-threshold (CT) values were compared for genes with a   2-fold increase by Mann-Whitney *U* test. Number of samples and statistical analyses are indicated in each figure legend. Each sample was tested in duplicate. A *p* value of <0.05 was considered significant.

RESULTS

ECMO is associated with intestinal epithelial cell apoptosis

To investigate whether epithelial apoptosis plays an early and underlying role in gut mucosal injury during ECMO, we first examined tissue sections of the small intestine (jejunum and ileum) from sham- and ECMO-treated piglets. As shown in Fig. 1, nuclear morphological changes that are typically associated with apoptosis were notable in epithelial cells in ECMO- but not in the sham-treated intestine. After 2h of ECMO, nuclei near the villus tips showed condensation of chromatin into distinct clumps. In the crypts, a few nuclei showed chromatin condensation, fragmentation, or pyknosis (Fig. 1A, C). After 8h of ECMO, most villi were completely denuded of epithelium. Most of the crypt epithelial cells showed apoptotic changes. These findings contrasted with the sham intestine, which did not show such apoptotic changes (Fig. 1B, C). To determine whether these findings of gut epithelial injury in piglet ECMO were relevant to human infants receiving ECMO, we reviewed archived autopsy samples from neonates (n=10) who died during ECMO. Tissue sections from all the 10 autopsies showed severe epithelial exfoliation in the gastrointestinal tract. A representative photomicrograph from a full-term infant who was treated with ECMO for intractable pulmonary hypertension and died during treatment is depicted in Fig. 1D.

To confirm whether ECMO was associated with apoptosis in intestinal epithelial cells, we examined the nuclear morphology in DAPI-stained sections and also performed TUNEL staining. As shown in Fig. 1E, apoptotic changes were detectable after 2h of ECMO. Nuclear fragmentation was a frequent finding in epithelial cells near the villus tips, whereas crypt cells showed peripheral condensation of chromatin (***panel a***). These findings indicated

that the apoptotic changes were at a more advanced stage near villus tips than in the crypts. After 8h of ECMO, a majority of crypt epithelial cells showed chromatin condensation. We also compared the nuclear geometry in epithelial cells in sham and ECMO intestine using computational image analysis. ECMO was associated with a reduction in nuclear area (2286.36 ± 238.4 in sham *vs*. 1586.39 ± 106.89 square pixels in the ECMO intestine, *p* <0.05; ***panel b***). We computed a nuclear irregularity index (NII), which includes nuclear area, the ratio of its major and minor radii, ratio of its area to the area of its bounding box, ratio of its major and minimum radii, and nuclear roundness. ECMO was associated with lower NII values (7.59 ± 0.4 in sham intestine *vs*. 6.45 ± 0.3 in ECMO, *p* <0.05; ***panel c***). These findings were suggestive of early apoptosis, which is typically associated with nuclear condensation and increased regularity of the nuclear outline.

TUNEL staining further supported our findings of apoptotic changes in the epithelium. As shown in Fig. 2A, TUNEL[+] nuclei were seen all along the villus tip and in some crypt cells at the 2h time-point. Finally, to confirm that epithelial apoptosis preceded villous damage during ECMO, we scored serial tissue sections for the severity of epithelial apoptosis and the severity of villous damage. Changes limited to villus tips received a score of 1, whereas involvement of the entire crypt-villus axis was scored as 4. As depicted in Fig. 2B, apoptosis scores increased before the onset of villous damage after 2h of ECMO.

Plasma I-FABP concentrations are increased during ECMO

Because swelling of villus tips and exfoliation of epithelial cells from villi can be a part of the post-mortem/autolytic changes in the intestine,[13, 14] we sought additional evidence that epithelial injury we noted in the ECMO intestine occurred while the animal was alive and during ECMO. Tissue sections were carefully screened and confirmed to be negative for other signs of autolysis such as hemolysis of red blood cells and the loss of differential staining in various layers. To investigate whether epithelial cell death occurred during ECMO, we measured serial plasma concentrations of I-FABP, a cytosolic protein uniquely located in mature enterocytes and a sensitive biochemical marker of early gut mucosal injury. As depicted in Fig. 3, I-FABP levels started rising soon after the initiation of ECMO and increased progressively during the 8h ECMO run.

ECMO activates the extrinsic pathway of apoptosis in intestinal epithelial cells

We next investigated the mechanism by which gut epithelial cells undergo apoptosis during ECMO. To determine the signaling pathway(s) involved in this process, we immunostained the sham and ECMO intestine for cleaved caspase-8, which is typically associated with the extrinsic, death receptor-linked pathway, and cleaved caspase-9, which is involved in the mitochondrial-related intrinsic pathway. We detected prominent epithelial immunoreactivity for cleaved caspase-8, but not cleaved caspase-9, in the ECMO intestine. The sham intestine did not stain for either of the two markers (Fig. 4A). To confirm these findings, we performed Western blots on tissue samples from sham and ECMO intestine. Unlike sham, ECMO intestine showed increased expression of the intermediate form of caspase-8, p43/p41, and of the active, cleaved fragment, p18 (Fig. 4B). There was no change in the full-length caspase-9 protein or its active p35 fragment.

ECMO induces fas ligand expression in the intestinal mast cells

To investigate the mechanisms underlying the activation of caspase-8 in the intestinal epithelium during ECMO, we first used RT-qPCR to measure the gene expression of death receptor ligands that are known to be associated with gut mucosal injury and have been characterized in swine. As depicted in Fig. 5A, ECMO was associated with increased expression of *fas* ligand/TNF superfamily, member 6 (TNFSF6), TNF-related apoptosis-inducing ligand (TRAIL)/TNFSF10, and TNF/TNFSF2. We have previously described increased expression of TNF during ECMO. There was also a trend towards increased CD40 ligand/TNFSF5 that did not reach significance. In the present study, we focused on *fas* ligand in subsequent experiments.

To identify the cellular source(s) of *fas* ligand in the intestine during ECMO, we next performed immunohistochemistry on tissue sections from the sham and ECMO intestine. As shown in Fig. 5B, ECMO was associated with increased immunoreactivity for *fas* ligand in *lamina propria* mast cells, which were identifiable by their prominent cytoplasmic granules and positive staining for *c*-kit/CD117. Consistent with the hypothesis that *fas* ligand promotes epithelial apoptosis during ECMO, many c-kit/CD117$^+$ *fas* ligand$^+$ mast cells could be identified in close proximity to epithelial nuclei that showed morphological changes of apoptosis (Fig. 5C).

P38 MAPK drives fas ligand expression in mast cells in the ECMO intestine

To determine the mechanisms driving *fas* ligand expression in intestinal mast cells, we focused on the role of p38 mitogen-activated protein kinase. Existing data implicate p38 activation in a wide range of mast cell functions, including differentiation, inflammatory activation, and degranulation.[15, 16] We first measured phospho-p38 expression in mast cells isolated from the sham and ECMO intestine by flow cytometry (Fig. 6A). This antibody detects p38 that is dual phosphorylated at the thr180 and tyr182 residues. Consistent with these findings, phospho-p38 was immunolocalized in c-kit/CD117$^+$ mast cells in ECMO, but not in the sham intestine (Fig. 6B).

We have previously demonstrated that ECMO is associated with epithelial barrier dysfunction and bacterial translocation.[7] Based on these observations, we hypothesized that increased exposure to bacterial products can induce p38-mediated *fas* ligand expression in intestinal mast cells during ECMO. To investigate this possibility, we treated mast cells from the normal piglet intestine with *E. coli* LPS *in vitro*, and as shown in Western blots in Fig. 6C, LPS promoted p38 phosphorylation in these cells. LPS also increased *fas* ligand expression in mast cells, which was blocked by prior exposure to SB202190, a specific small molecule inhibitor of p38 MAPK (Fig. 6D). These data emphasize the role of p38-mediated signaling in the induction of *fas* ligand in mast cells.

DISCUSSION

We present a detailed investigation into the timing and mechanisms of gut epithelial injury during ECMO. In our piglet model of ECMO, epithelial apoptosis preceded villous damage and continued throughout the 8h course of the study. We show that the extrinsic apoptotic

pathway is at play in the epithelium, with evidence of increased expression of *fas* ligand and related death receptor ligands by *lamina propria* mast cells. Finally, we show that the ECMO was associated with activation of p38 MAPK in intestinal mast cells, which induced *fas* ligand expression in these cells. To our knowledge, this is the first study to investigate the mechanisms of gut epithelial injury in extracorporeal circulation.

In our piglet model, we detected extensive epithelial apoptosis after 2h of ECMO. We chose a cautious approach and sought multiple lines of evidence to confirm apoptotic changes because of concerns that in necrotic tissue injury, a single test such as TUNEL may not be adequate for accurate estimation of apoptosis.[17–20] Although the effects of extracorporeal circulation on the gut epithelium are not well-documented, increased epithelial apoptosis has been described in diverse gastrointestinal conditions such as ischemia-reperfusion (I/R) injury, necrotizing enterocolitis (NEC), infectious diarrhea, celiac disease, and inflammatory bowel disease.[11, 21–24] Interestingly, epithelial apoptosis in our model of piglet ECMO followed a pattern similar to intestinal I/R injury, where apoptotic changes occur earlier and are more extensive at villus tips than in the crypts. Similar to the clinical experience during human ECMO, piglets receiving ECMO frequently developed tachycardia and hypotension within 1–2h of initiation of the procedure, which responded to intravenous fluid boluses.[6] In these animals, even though hemodynamic parameters were maintained in the normal range with aggressive fluid resuscitation, subclinical gut ischemia due to the redistribution of blood flow to vital organs is plausible. Besides direct effects of extracorporeal circulation, I/R is also a plausible contributor to bowel injury during both ECMO and CPB because both modalities are often used in infants with cardiopulmonary failure who may have had varying degrees of intestinal hypoperfusion prior to the initiation of the procedure. During venoarterial ECMO, significant hemodynamic changes have been documented due to the loss of pulsatile blood flow and during times when the bridge between the venous drainage and the infusion tubing is opened.[25] During CPB, intra-operative cardioplegia, aortic cross-clamping, hypothermia, and hemodilution can add to the risk of intestinal I/R.[26–29] Although the pathophysiological significance of epithelial apoptosis in the ECMO-related bowel injury remains uncertain, it is known to play a central role in intestinal I/R injury; in preclinical models, strategies to prevent gut epithelial apoptosis such as pre-treatment with caspase inhibitors or gut epithelial-specific over-expression of bcl-2 have been shown to reduce the severity of histopathological damage.[30]

ECMO was associated with increased expression of cleaved caspase-8 in intestinal epithelium, indicating that the extrinsic pathway of apoptosis was activated in these cells. Caspase-8 is a cysteine protease that initiates apoptosis in response to cell surface receptors of the TNF receptor superfamily called the death receptors (DRs).[31] To trigger cell death, DRs recruit an adaptor protein, the *fas*-associated protein with a death domain (FADD), which then activates the caspase-8 pro-enzyme, leading to activation of downstream caspases 3, 6, and 7, and apoptosis.[32] In a previous report, we had shown that ECMO was associated with activation of intestinal mast cells, which released pre-formed TNF.[6] However, when all the DR ligands were measured simultaneously in the present study, *fas* ligand was the most highly-expressed gene in this superfamily. Besides direct activation of DR-mediated signaling, DR ligands can also activate the extrinsic apoptotic pathway

indirectly in epithelial cells through cytoskeletal condensation and disruption of the tight junctions. Dissolution of tight junctions can release occludin, which can serve as a non-canonical DR ligand to activate the extrinsic pathway.[33]

Fas ligand has been implicated in gut epithelial apoptosis in several diseases, including I/R, Crohn's disease, ulcerative colitis, celiac disease, and graft *vs*. host disease.[34, 35] *Fas* ligand ligates its cognate receptor, *fas*/CD95, which is constitutively expressed on the basolateral surface of epithelial cells.[23, 36, 37] Following ligation of *fas*, caspase-8 activation results in the formation of a hetero-tetramer comprised of two units each of the enzymatically-active caspase-8 fragments, p18 and p10.[31] Two pathways have been described[38]: the type I pathway is invoked by membrane-bound *fas* ligand and results in the formation of relatively copious amounts of the caspase-8 hetero-tetramers. The type II pathway overlaps with the intrinsic apoptotic pathway and is often seen in T-lymphoblasts such as Jurkat cells, where membrane-bound or soluble *fas* ligand activates the pro-apoptotic protein *bid* (BH3 interacting-domain death agonist), which results in mitochondrial damage and apoptosis.[39] Intestinal epithelial cells generally display type I-like characteristics with activation with formation of large amounts of the active caspase-8 fragments.[40] However, an important caveat for the role of *fas* ligand is that despite its identification as the trigger for epithelial apoptosis in various diseases, its pathophysiological significance in gut mucosal injury remains unproven because mice with deficiencies in *fas* and *fas* ligand do not seem to be protected in chemical colitis models.[41]

We have identified mast cells as the primary cellular source of *fas* ligand in the ECMO intestine. These findings are consistent with our previous observations that ECMO is associated with degranulation and activation of intestinal mast cells, which rapidly release inflammatory mediators such as TNF, tryptase, and chymase locally and into the circulation.[6, 7] Mast cells also release inflammatory mediators, including *fas* ligand, in exosomes.[42] Intestinal mast cells are increasingly recognized as a major source of pre-formed inflammatory mediators in SIRS in diverse settings such as in Gram-negative and Gram-positive bacterial sepsis, peritonitis, severe alveolar hypoxia, and portal hypertension.[43–47] Although the initial trigger for intestinal epithelial cell apoptosis in our model remains unclear, we speculate that pre-formed stores of *fas* ligand in mast cells may play a role. Once the epithelial barrier is disrupted, increased exposure to bacterial products can explain p38-mediated *fas* ligand expression in mast cells, and a feed-forward cycle of epithelial damage, bacterial translocation, and mast cell activation (Fig. 7).

Elucidation of the inflammatory pathways involved in extracorporeal circulation-related SIRS is a critical step in the development of effective anti-inflammatory therapies. Extracorporeal circulation-related SIRS cannot be prevented merely by improvements in the membrane oxygenator or the circuit. Physical characteristics of the ECMO/CPB circuit such as fluid dynamics, blood volume to surface area ratio, and the material's affinity for fibrinogen determine its propensity for contact activation of inflammatory pathways.[48] Although smoother circuits can be designed, the structure of the membrane oxygenator calls for conflicting profiles - the necessity for the gas exchange obligates thin blood films and turbulence, factors that also favor contact activation. Thus, even though improved silicone oxygenators have shown modest benefit in reducing platelet and contact activation, these

improvements face a mathematical bottleneck where reduction in turbulence and blood surface interaction compete with the gas exchange capacity of the oxygenator.[49] We have identified caspase-8-mediated epithelial apoptosis and intestinal mast cells as potentially-important pathophysiological mediators in ECMO-related bowel injury, which can accentuate the SIRS through increased systemic exposure to bacterial products. Further study is needed in patients receiving ECMO/CPB to determine the kinetics and significance of these events during human ECMO.

Acknowledgments

Abbreviations

DAPI	4′,6-diamidino-2-phenylindole
CPB	Cardiopulmonary bypass
ELISA	Enzyme-linked immunosorbent assay
ECMO	Extracorporeal membrane oxygenation
I-FABP	Intestinal-fatty acid binding protein
LPS	Lipopolysaccharide
MAPK	Mitogen-activated protein kinase
PBS	Phosphate-buffered saline
RT-qPCR	Reverse transcriptase-quantitative polymerase chain reaction
SIRS	Systemic inflammatory response syndrome
TUNEL	Terminal deoxynucleotidyl transferase-mediated dUTP Nick End Labeling
TNF	Tumor necrosis factor
TNFSF	TNF superfamily member
TRAIL	TNF-related apoptosis-inducing ligand
TWEAK	TNF-related weak inducer of apoptosis

References

1. Chen Q, Yu W, Shi J, et al. The effect of venovenous extra-corporeal membrane oxygenation (ECMO) therapy on immune inflammatory response of cerebral tissues in porcine model. Journal of cardiothoracic surgery. 2013; 8(1):186. [PubMed: 23985062]

2. Halter J, Steinberg J, Fink G, et al. Evidence of systemic cytokine release in patients undergoing cardiopulmonary bypass. The Journal of extra-corporeal technology. 2005; 37(3):272–277. [PubMed: 16350379]

3. Mildner RJ, Taub N, Vyas JR, et al. Cytokine imbalance in infants receiving extracorporeal membrane oxygenation for respiratory failure. Biol Neonate. 2005; 88(4):321–327. [PubMed: 16113527]

4. Ichiba S, Bartlett RH. Current status of extracorporeal membrane oxygenation for severe respiratory failure. Artificial organs. 1996; 20(2):120–123. [PubMed: 8712954]

5. Paden ML, Conrad SA, Rycus PT, Thiagarajan RR, Registry E. Extracorporeal Life Support Organization Registry Report 2012. ASAIO journal. 2013; 59(3):202–210. [PubMed: 23644605]

6. Mc ILwain RB, Timpa JG, Kurundkar AR, et al. Plasma concentrations of inflammatory cytokines rise rapidly during ECMO-related SIRS due to the release of preformed stores in the intestine. Laboratory investigation; a journal of technical methods and pathology. 2010; 90(1):128–139.

7. Kurundkar AR, Killingsworth CR, McIlwain RB, et al. Extracorporeal membrane oxygenation causes loss of intestinal epithelial barrier in the newborn piglet. Pediatr Res. 2010; 68(2):128–133. [PubMed: 20442689]

8. Kerr JF, Wyllie AH, Currie AR. Apoptosis: a basic biological phenomenon with wide-ranging implications in tissue kinetics. British journal of cancer. 1972; 26(4):239–257. [PubMed: 4561027]

9. Filippi-Chiela EC, Oliveira MM, Jurkovski B, Callegari-Jacques SM, da Silva VD, Lenz G. Nuclear morphometric analysis (NMA): screening of senescence, apoptosis and nuclear irregularities. PLoS One. 2012; 7(8):e42522. [PubMed: 22905142]

10. Schneider CA, Rasband WS, Eliceiri KW. NIH Image to ImageJ: 25 years of image analysis. Nature methods. 2012; 9(7):671–675. [PubMed: 22930834]

11. Jilling T, Lu J, Jackson M, Caplan MS. Intestinal epithelial apoptosis initiates gross bowel necrosis in an experimental rat model of neonatal necrotizing enterocolitis. Pediatr Res. 2004; 55(4):622–629. [PubMed: 14764921]

12. Sellge G, Bischoff SC. Isolation, culture, and characterization of intestinal mast cells. Methods Mol Biol. 2006; 315:123–138. [PubMed: 16110154]

13. Pearson GR, Logan EF. Scanning electron microscopy of early postmortem artefacts in the small intestine of a neonatal calf. British journal of experimental pathology. 1978; 59(5):499–503. [PubMed: 718801]

14. Thorpe E, Thomlinson JR. Autolysis and post-mortem bacteriological changes in the alimentary tract of the pig. The Journal of pathology and bacteriology. 1967; 93(2):601–610. [PubMed: 4861402]

15. Zhang C, Baumgartner RA, Yamada K, Beaven MA. Mitogen-activated protein (MAP) kinase regulates production of tumor necrosis factor-alpha and release of arachidonic acid in mast cells. Indications of communication between p38 and p42 MAP kinases. The Journal of biological chemistry. 1997; 272(20):13397–13402. [PubMed: 9148963]

16. Feoktistov I, Goldstein AE, Biaggioni I. Role of p38 mitogen-activated protein kinase and extracellular signal-regulated protein kinase kinase in adenosine A2B receptor-mediated interleukin-8 production in human mast cells. Molecular pharmacology. 1999; 55(4):726–734. [PubMed: 10101031]

17. Kelly KJ, Sandoval RM, Dunn KW, Molitoris BA, Dagher PC. A novel method to determine specificity and sensitivity of the TUNEL reaction in the quantitation of apoptosis. American journal of physiology Cell physiology. 2003; 284(5):C1309–1318. [PubMed: 12676658]

18. Tamura T, Said S, Lu W, Neufeld D. Specificity of TUNEL method depends on duration of fixation. Biotechnic & histochemistry: official publication of the Biological Stain Commission. 2000; 75(4):197–200. [PubMed: 10999571]

19. Zhao J, Schmid-Kotsas A, Gross HJ, Gruenert A, Bachem MG. Sensitivity and specificity of different staining methods to monitor apoptosis induced by oxidative stress in adherent cells. Chinese medical journal. 2003; 116(12):1923–1929. [PubMed: 14687485]

20. Yasuhara S, Zhu Y, Matsui T, et al. Comparison of comet assay, electron microscopy, and flow cytometry for detection of apoptosis. The journal of histochemistry and cytochemistry: official journal of the Histochemistry Society. 2003; 51(7):873–885. [PubMed: 12810838]

21. Ramachandran A, Madesh M, Balasubramanian KA. Apoptosis in the intestinal epithelium: its relevance in normal and pathophysiological conditions. Journal of gastroenterology and hepatology. 2000; 15(2):109–120. [PubMed: 10735533]

22. Iwamoto M, Koji T, Makiyama K, Kobayashi N, Nakane PK. Apoptosis of crypt epithelial cells in ulcerative colitis. J Pathol. 1996; 180(2):152–159. [PubMed: 8976873]

23. Ciccocioppo R, Di Sabatino A, Parroni R, et al. Increased enterocyte apoptosis and Fas-Fas ligand system in celiac disease. American journal of clinical pathology. 2001; 115(4):494–503. [PubMed: 11293896]

24. Chen LW, Egan L, Li ZW, Greten FR, Kagnoff MF, Karin M. The two faces of IKK and NF-kappaB inhibition: prevention of systemic inflammation but increased local injury following intestinal ischemia-reperfusion. Nature medicine. 2003; 9(5):575–581.

25. Van Heijst A, Liem D, Van Der Staak F, et al. Hemodynamic changes during opening of the bridge in venoarterial extracorporeal membrane oxygenation. Pediatric critical care medicine: a journal of the Society of Critical Care Medicine and the World Federation of Pediatric Intensive and Critical Care Societies. 2001; 2(3):265–270. [PubMed: 12793953]

26. Peek GJ, Firmin RK. The inflammatory and coagulative response to prolonged extracorporeal membrane oxygenation. ASAIO J. 1999; 45(4):250–263. [PubMed: 10445729]

27. Caputo M, Bays S, Rogers CA, et al. Randomized comparison between normothermic and hypothermic cardiopulmonary bypass in pediatric open-heart surgery. Ann Thorac Surg. 2005; 80(3):982–988. [PubMed: 16122470]

28. Asimakopoulos G. Systemic inflammation and cardiac surgery: an update. Perfusion. 2001; 16(5): 353–360. [PubMed: 11565890]

29. Brix-Christensen V. The systemic inflammatory response after cardiac surgery with cardiopulmonary bypass in children. Acta Anaesthesiol Scand. 2001; 45(6):671–679. [PubMed: 11421823]

30. Coopersmith CM, O'Donnell D, Gordon JI. Bcl-2 inhibits ischemia-reperfusion-induced apoptosis in the intestinal epithelium of transgenic mice. The American journal of physiology. 1999; 276(3 Pt 1):G677–686. [PubMed: 10070044]

31. Hoffmann JC, Pappa A, Krammer PH, Lavrik IN. A new C-terminal cleavage product of procaspase-8, p30, defines an alternative pathway of procaspase-8 activation. Molecular and cellular biology. 2009; 29(16):4431–4440. [PubMed: 19528225]

32. Cabal-Hierro L, Lazo PS. Signal transduction by tumor necrosis factor receptors. Cell Signal. 2012; 24(6):1297–1305. [PubMed: 22374304]

33. Beeman NE, Baumgartner HK, Webb PG, Schaack JB, Neville MC. Disruption of occludin function in polarized epithelial cells activates the extrinsic pathway of apoptosis leading to cell extrusion without loss of transepithelial resistance. BMC cell biology. 2009; 10:85. [PubMed: 20003227]

34. An S, Hishikawa Y, Koji T. Induction of cell death in rat small intestine by ischemia reperfusion: differential roles of Fas/Fas ligand and Bcl-2/Bax systems depending upon cell types. Histochemistry and cell biology. 2005; 123(3):249–261. [PubMed: 15765213]

35. Inagaki-Ohara K, Nishimura H, Sakai T, Lynch DH, Yoshikai Y. Potential for involvement of Fas antigen/Fas ligand interaction in apoptosis of epithelial cells by intraepithelial lymphocytes in murine small intestine. Laboratory investigation; a journal of technical methods and pathology. 1997; 77(5):421–429.

36. Abreu MT, Palladino AA, Arnold ET, Kwon RS, McRoberts JA. Modulation of barrier function during Fas-mediated apoptosis in human intestinal epithelial cells. Gastroenterology. 2000; 119(6): 1524–1536. [PubMed: 11113074]

37. Ueyama H, Kiyohara T, Sawada N, et al. High Fas ligand expression on lymphocytes in lesions of ulcerative colitis. Gut. 1998; 43(1):48–55. [PubMed: 9771405]

38. Jost PJ, Grabow S, Gray D, et al. XIAP discriminates between type I and type II FAS-induced apoptosis. Nature. 2009; 460(7258):1035–1039. [PubMed: 19626005]

39. Kantari C, Walczak H. Caspase-8 and bid: caught in the act between death receptors and mitochondria. Biochimica et biophysica acta. 2011; 1813(4):558–563. [PubMed: 21295084]

40. Pinkoski MJ, Brunner T, Green DR, Lin T. Fas and Fas ligand in gut and liver. Am J Physiol Gastrointest Liver Physiol. 2000; 278(3):G354–366. [PubMed: 10712254]

41. Park SM, Chen L, Zhang M, Ashton-Rickardt P, Turner JR, Peter ME. CD95 is cytoprotective for intestinal epithelial cells in colitis. Inflamm Bowel Dis. 2010; 16(6):1063–1070. [PubMed: 20049944]

42. Zuccato E, Blott EJ, Holt O, et al. Sorting of Fas ligand to secretory lysosomes is regulated by mono-ubiquitylation and phosphorylation. Journal of cell science. 2007; 120(Pt 1):191–199. [PubMed: 17164290]

43. Mallen-St Clair J, Pham CT, Villalta SA, Caughey GH, Wolters PJ. Mast cell dipeptidyl peptidase I mediates survival from sepsis. J Clin Invest. 2004; 113(4):628–634. [PubMed: 14966572]

44. Sutherland RE, Olsen JS, McKinstry A, Villalta SA, Wolters PJ. Mast cell IL-6 improves survival from Klebsiella pneumonia and sepsis by enhancing neutrophil killing. J Immunol. 2008; 181(8): 5598–5605. [PubMed: 18832718]

45. Nautiyal KM, McKellar H, Silverman AJ, Silver R. Mast cells are necessary for the hypothermic response to LPS-induced sepsis. Am J Physiol Regul Integr Comp Physiol. 2009; 296(3):R595–602. [PubMed: 19109365]

46. Chao J, Wood JG, Gonzalez NC. Alveolar hypoxia, alveolar macrophages, and systemic inflammation. Respir Res. 2009; 10(1):54. [PubMed: 19545431]

47. Tang CW, Lan C, Liu R. Increased activity of the intestinal mucosal mast cells in rats with multiple organ failure. Chin J Dig Dis. 2004; 5(2):81–86. [PubMed: 15612663]

48. Hennessy VL Jr, Hicks RE, Niewiarowski S, Edmunds LH Jr, Colman RW. Function of human platelets during extracorporeal circulation. Am J Physiol. 1977; 232(6):H622–628. [PubMed: 18017]

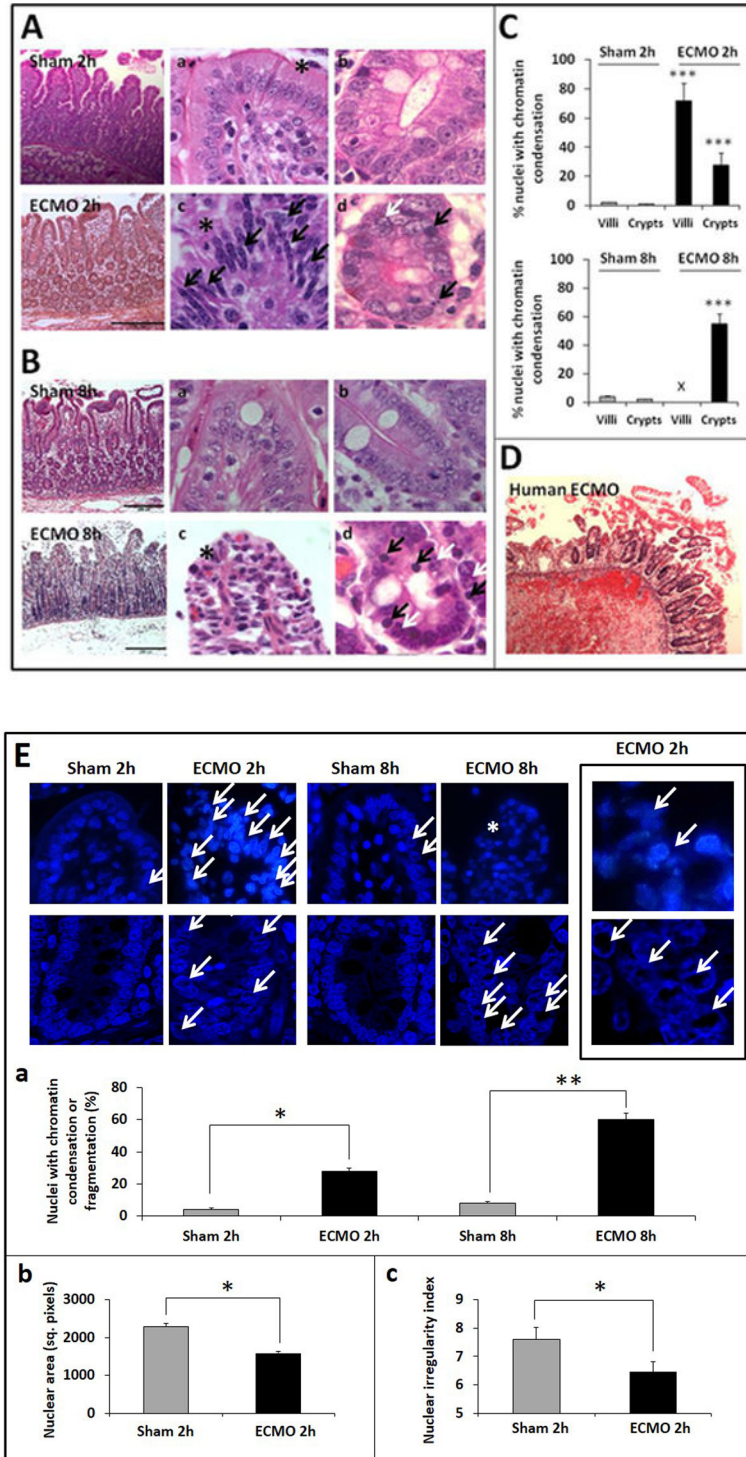49. Baier RE. The organization of blood components near interfaces. Ann N Y Acad Sci. 1977; 283:17–36.

Fig. 1. ECMO is associated with apoptotic changes in intestinal epithelial cells
A. Representative photomicrographs on the left show H&E-stained intestinal tissue (100×) from sham- and ECMO-treated piglets after 2h of treatment. Photomicrographs (1000×) on the right show representative (a) sham villus; (b) sham crypt; (c) ECMO villus; and the (d) ECMO crypt. Many epithelial cells showed changes in nuclear morphology suggestive of

apoptosis, such as clumping of chromatin, pyknosis, or nuclear fragmentation (black arrows), or peripheral condensation of chromatin (white arrows). **B.** Tissues obtained after 8h of ECMO (ordered similarly as in panel A) showed extensive epithelial exfoliation from villus tips (asterisk). In the crypts, many epithelial cells showed pyknosis (black arrows) or peripheral condensation of chromatin (white arrows). **C.** Bar diagrams (means ± standard errors) show the percentage of epithelial nuclei with chromatin condensation in the sham and ECMO intestine after 2h (top) and 8h (bottom). In the 8h intestine, no data are shown for villi because of extensive exfoliation of the villus epithelium. **D.** H&E-stained intestinal tissue section (100×) from a full-term, 21-day old human infant who died during ECMO shows similar loss of epithelium. **E.** Representative fluorescence photomicrographs (630x) show nuclear staining with DAPI (blue) in the sham and ECMO intestine after 2h and 8h of treatment. Arrows indicate nuclei with chromatin fragmentation or peripheral condensation ('signet ring' appearance). The 8h ECMO villus was denuded of epithelium (asterisk). High-magnification photomicrographs (2000x, in the box on right) highlight nuclei that have undergone fragmentation (top) and peripheral chromatin condensation. Below, bar diagrams (means ± SE) depict (a) percentage of epithelial nuclei with chromatin condensation or fragmentation in the sham or ECMO intestine at 2h and 8h; (b) nuclear area in the sham *vs.* ECMO intestine after 2h of treatment; and (c) nuclear irregularity index in the sham *vs.* ECMO intestine after 2h.
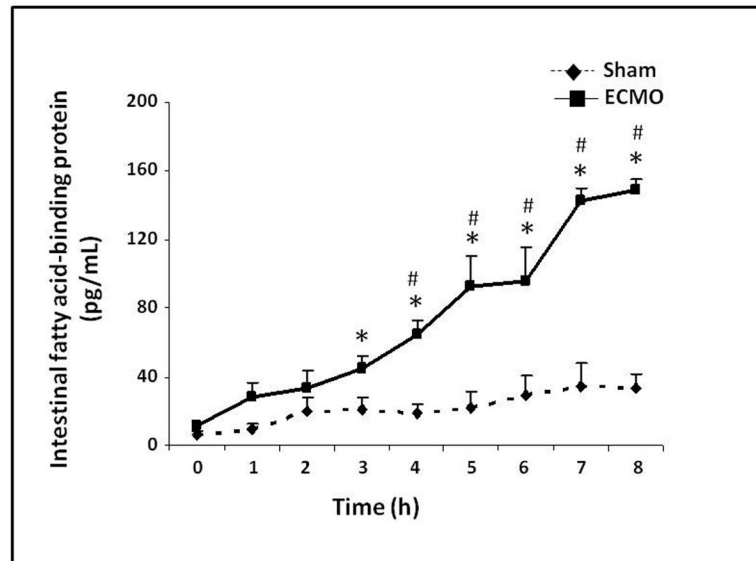
Fig. 2. Epithelial cell apoptosis precedes villus injury during ECMO
A. Representative photomicrographs show TUNEL staining (green) that confirmed increased intestinal epithelial cell apoptosis in the ECMO intestine compared to sham after 2h of treatment (arrows); *B.* Bar diagrams (means ± standard error) show epithelial cell apoptosis (score) and the villus disruption (score) in serial sections from the sham- and ECMO-treated intestine. Data represent n = 5 animals per group. * indicates *p*<0.05, ** *p*<0.01, and *** *p*<0.001.

Fig. 3. Circulating intestinal fatty acid-binding protein concentrations are increased during ECMO

Line diagram (means ± standard error) shows plasma concentrations of intestinal fatty-acid binding protein in sham- and ECMO-treated piglets. Data represent n = 8 animals per group. * indicates $p<0.05$ compared to sham (Kruskal-Wallis H test); # indicates $p<0.05$ compared to baseline measurement in ECMO animals (repeated measures analysis by Friedman test).
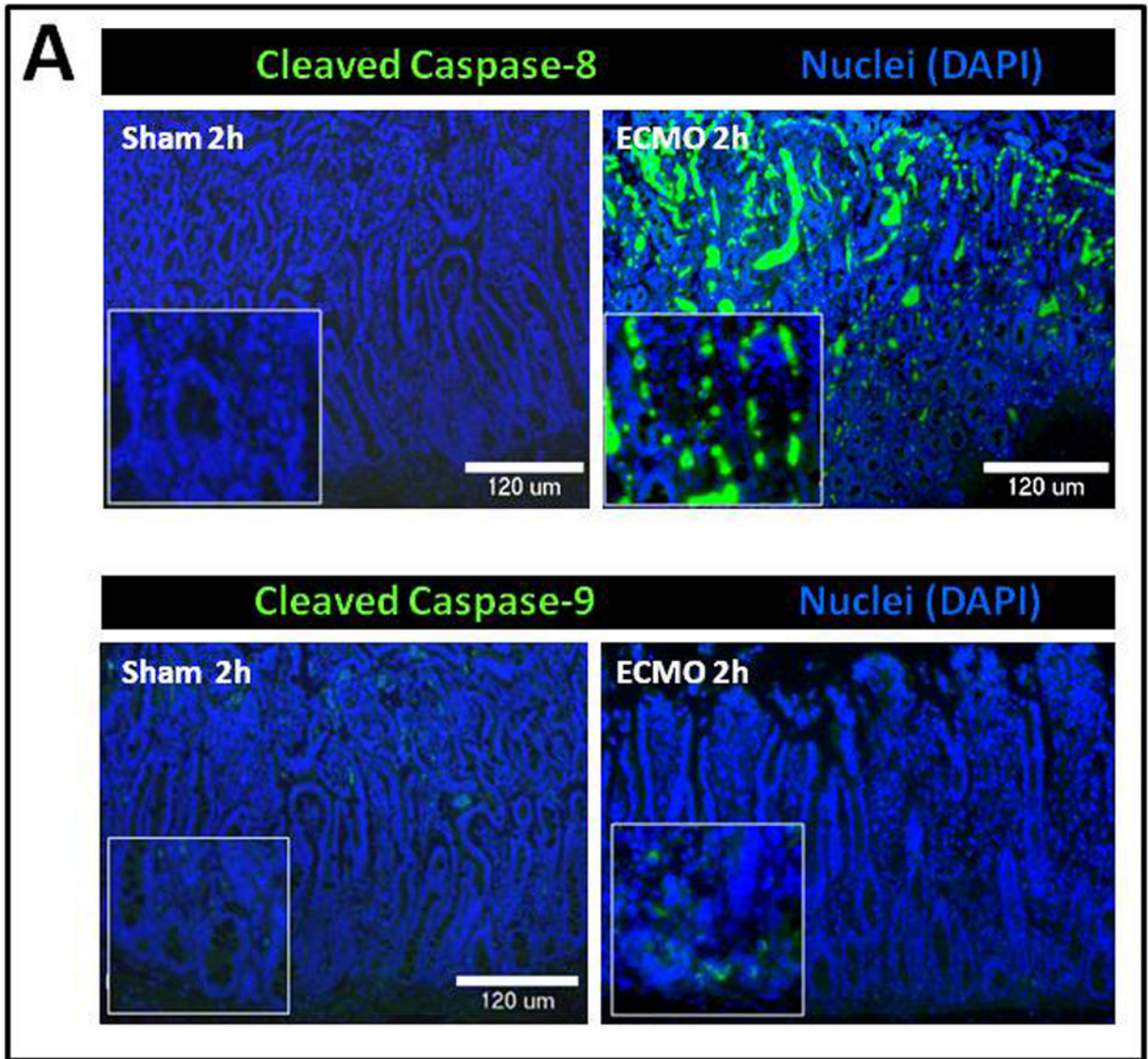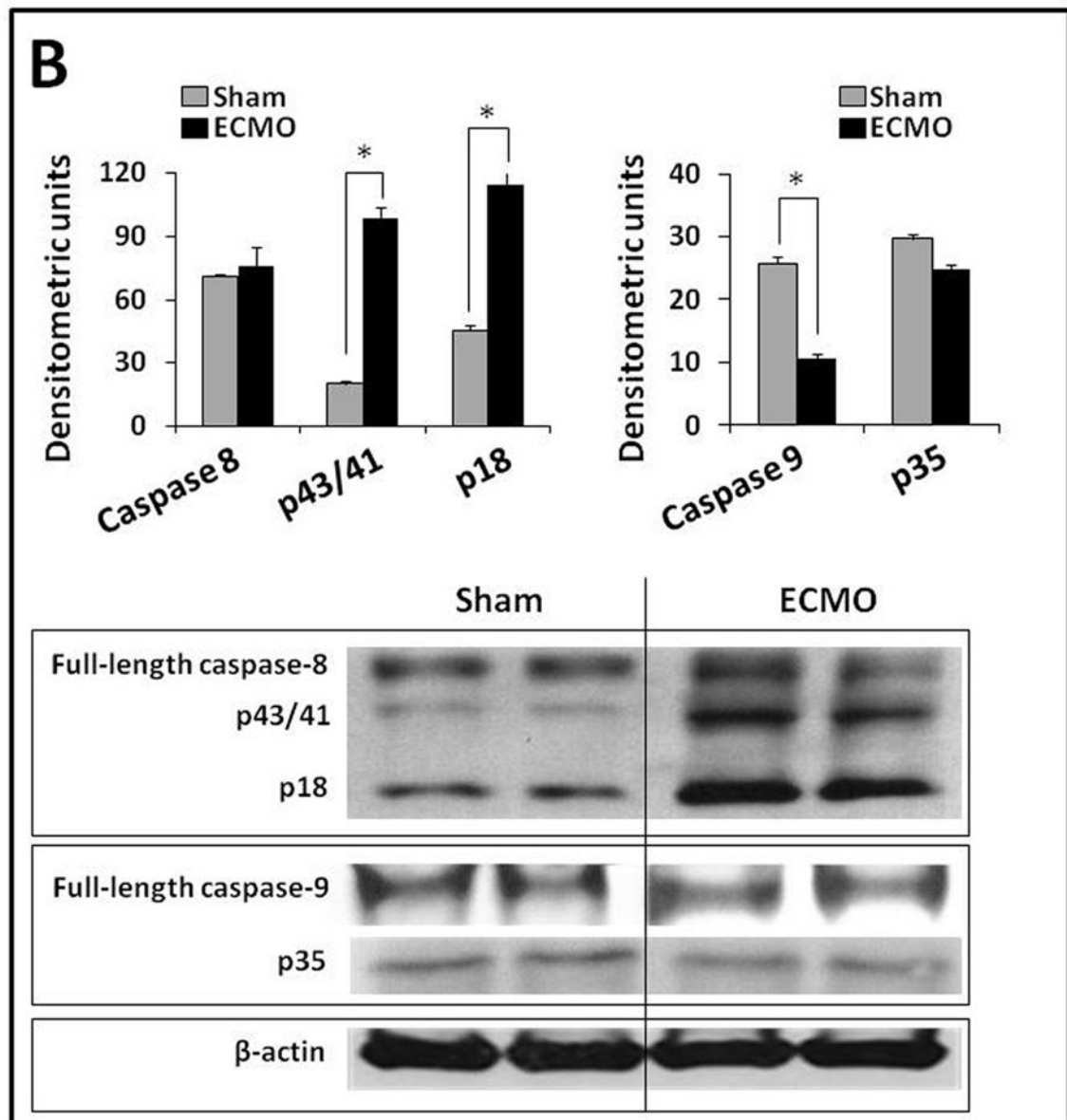
Fig. 4. ECMO activates the extrinsic pathway of apoptosis in intestinal epithelial cells
A. Representative fluorescence photomicrographs from sham- and ECMO-treated piglet intestine after 2h of treatment show immunoreactivity for cleaved caspase-8 (***panel A***), but not for cleaved caspase-9 (***panel B***), in intestinal epithelial cells. Nuclear staining (blue) was obtained with DAPI. *B*. Representative Western blots show cleaved caspase-8 and cleaved caspase-9 expression in the sham and ECMO intestine after treatment for 2h. *Upper box:* ECMO intestine showed increased expression of the intermediate form of caspase-8, p43/p41, and of the active, cleaved fragment, p18. *Middle box:* ECMO was associated with caspase-9, with no change in cleaved caspase-9 (p35). *Lower box:* β-actin expression (housekeeping gene). Bar diagrams (means ± SE) show summarized densitometric data. Data represent n = 5 animals per group. * indicates p<0.05.
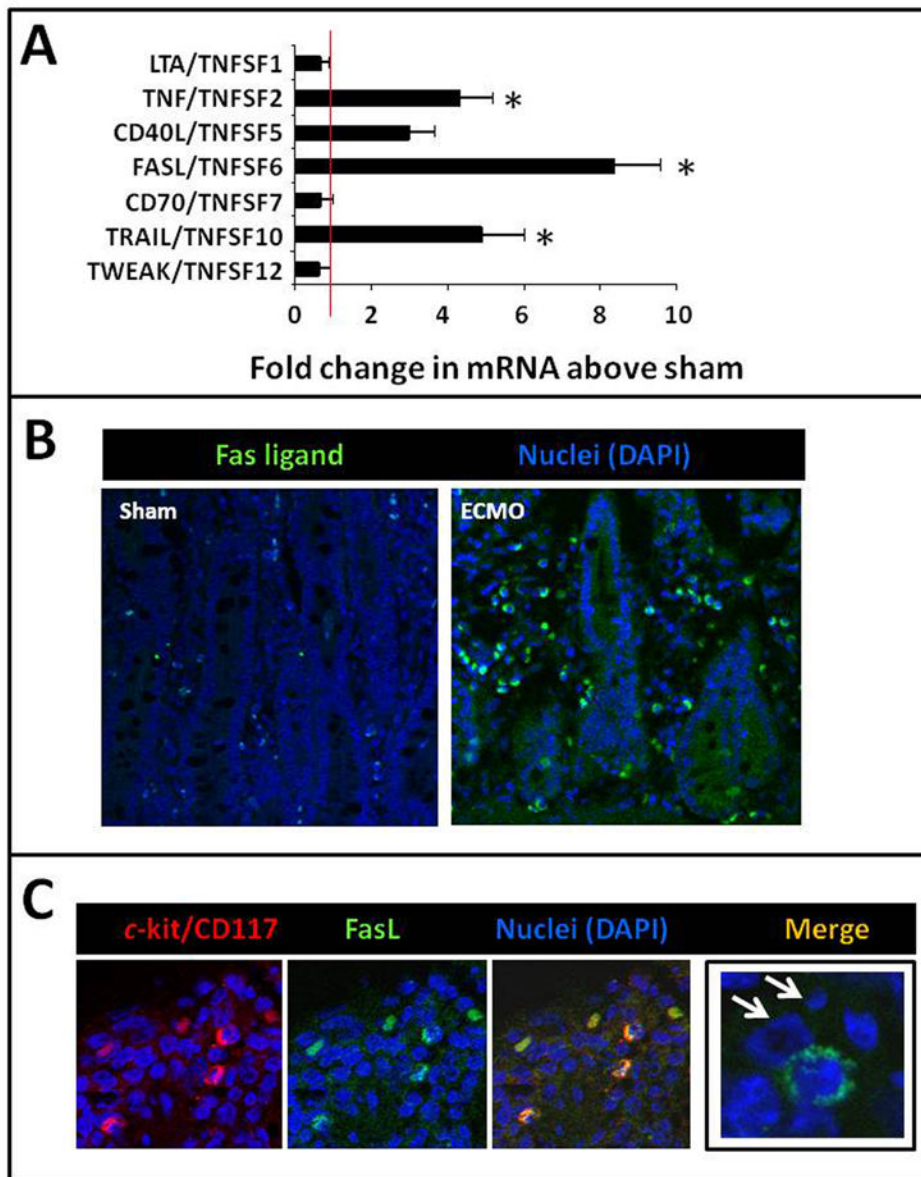
Fig. 5. ECMO induces *fas* ligand expression in the intestinal mast cells
A. Bar diagram (means ± SE) shows fold change in mRNA expression of major death receptor ligands in sham- and ECMO-treated porcine intestine after treatment for 2h. ECMO was associated with a significant increase in *fas* ligand, TRAIL, and TNF expression. ***B***. Fluorescence photomicrographs (100×) show increased immunoreactivity for *fas* ligand (green) in the ECMO intestine. Nuclear staining (blue) was obtained with DAPI. ***C.*** Fluorescence photomicrographs (400×) localize *fas* ligand (green) in *c*-kit/CD117+ mast cells (red) present in the *lamina propria*. Inset shows a *fas* ligand-expressing mast cell in close proximity to an apoptotic epithelial cell (arrows). Data are representative of n = 5 animals in sham and ECMO groups. * indicates p<0.05.

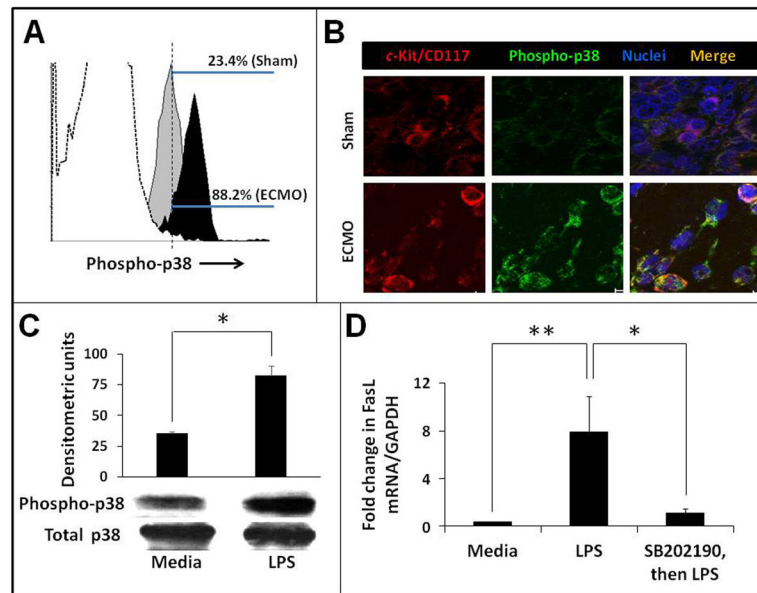**Fig. 6. Activation of p38 MAPK plays a key role in *fas* ligand production in mast cells in the ECMO intestine**

A. ECMO is associated with increased phospho-p38 expression in intestinal mast cells. Representative histograms obtained by FACS analysis show phospho-p38 expression in intestinal mast cells from sham and ECMO piglets, obtained after 2h of treatment. ***B.*** Fluorescent photomicrographs (630×) show that phospho-p38 (green) was immunolocalized in c-kit/CD117+ mast cells (red). Data represent n= 5 animals in sham and ECMO groups. ***C***. Representative Western blots show that LPS-treatment of mast cells isolated from normal piglet intestine *ex vivo* promotes p38 phosphorylation in these cells. Bar diagram (means ± SE) shows summarized densitometric data. ***D***. Bar diagram (means ± SE) shows fold change in fas ligand mRNA expression in intestinal mast cells (isolated from normal piglet intestine) in the native state, after treatment with LPS (1 μg/mL), and with SB202190 (1 μM) prior to LPS-treatment. Data represent 3 separate experiments. * indicates $p < 0.05$, ** indicates $p < 0.01$.

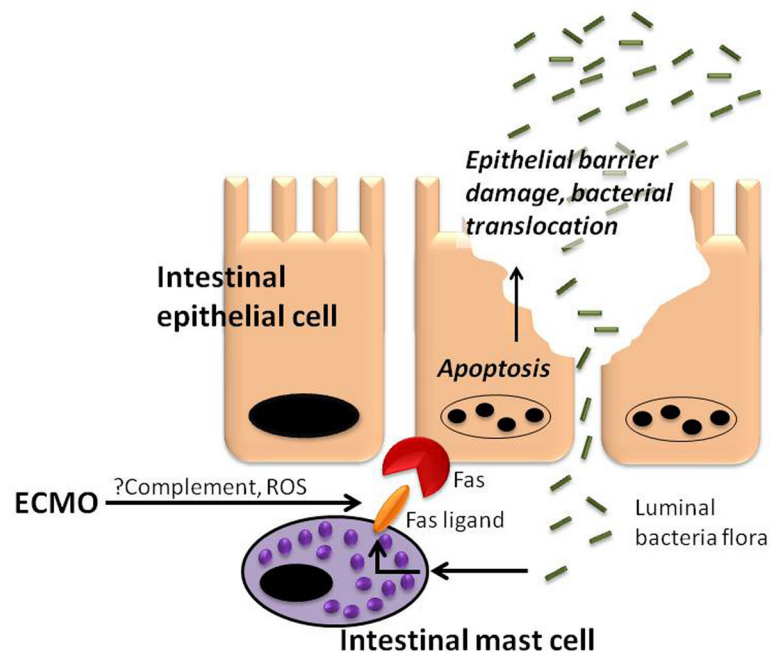**Fig. 7. Schematic showing the proposed pathophysiological model for intestinal epithelial cell apoptosis during ECMO**
ECMO-induced mast cell degranulation releases *fas* ligand, which triggers intestinal epithelial cell apoptosis, epithelial barrier disruption, and bacterial translocation. These bacterial products then activate p38 MAPK to promote sustained expression of *fas* ligand in mast cells, thereby setting up a feed-forward cycle of epithelial damage, bacterial translocation, and mast cell activation.

Table 1

Primer sequences used for real-time reverse transcriptase-PCR

mRNA	Forward primer	Reverse primer
TNFSF1	TTCCAACAGTCTCATCTTCC	ATCCTCAGCAGAGCATCC
TNFSF2	TGCCTTGGTTCAGATGTG	GAGGTTCAGCGATGTAGC
TNFSF5	GACAAGGAATCTATTACATCTACG	AGAGGCTGGCTATGAAGG
TNFSF6	CCTGTGTCTCCTTGTGATG	GATGATTCTGTATGCCTTTGG
TNFSF7	ACATCCAGGTGACATTGAC	TGAAAGTTGAGGCGTAGC
TNFSF10	GACCCAGCAATCCCACTC	CACACCTTCTTAATCTATTCATCC
TNFSF12	GCCTCTCCCTCCGTGTAG	GAGTTGTCAGGACCGATGG